Classical theory of second-harmonic generation from magnetic metamaterials

Yong Zeng[1,*], Walter Hoyer[2,†] , Jinjie Liu[1], Stephan W. Koch[2], Jerome V. Moloney[1]
1. Arizona Center for mathematical Sciences, University of Arizona, Tucson, Arizona 85721
2. Department of Physics and Material Sciences Center,
Philipps University, Renthof 5, D-35032 Marburg, Germany

Strong second-harmonic generation has recently been experimentally observed from metamaterials consisting of periodic arrays of metal split ring resonators with an effective negative magnetic permeability [Science, 313, 502 (2006)]. Because of the appearance of the fundamental plasmonic resonance, both electric and magnetic fields are strongly localized inside gap of the resonator, which in turn greatly enhances the conversion efficiency of second-harmonic generation. To explore the underlying physical mechanism, a classical model derived from microscopic theory is employed here. The quasi-free electrons inside the metal are approximated as a classical Coulomb-interacting electron gas, and their motion under the excitation of an external electromagnetic field is described by the cold-plasma wave equations. Through numerical simulations, it is demonstrated that the microscopic theory includes the dominant physical mechanisms both qualitatively and quantitatively. It is shown that, in contrast to previous interpretations, the dominant source term for second-harmonic generation results from *the convective derivative of the continuous electron current*.

PACS numbers: 42.70.-a, 52.35.Mw

Strong second-harmonic generation (SHG) from magnetic matematerials (MMs) has recently been experimentally observed [1, 2, 3]. Due to the periodic arrangement of artificial metallic subwavelength structures, such MMs possess plasmonic resonances as well as frequency regions with effective negative magnetic permeabilities [4, 5, 6, 7]. In particular, under the excitation with an external electromagnetic (EM) wave, quasi-free electrons inside MMs are coherently driven by the Lorentz force and form a circulating current. The current in turn generates an induced magnetic field pointing opposite to the original one. In a first explanation of the observed intensity dependence of the SHG on sample geometry and polarization direction of the exciting field, it has been assumed that the magnetic component of the Lorentz force provides the dominative second-order source [1, 2]. However, in a theoretical description of a classical Coulomb-interacting electron fluid, three different nonlinear source terms exist which can potentially contribute to the observed second-harmonic (SH) signal. In this Letter, we derive and numerically solve the corresponding equations and study the underlying physical mechanism of SHG theoretically. We show that our model gives good agreement with the experimentally observed SH strengths and thus catches the dominant physical mechanism. A switch-off analysis furthermore demonstrates that the dominant SH source can be traced back to the convective derivative of the continuum generalization of Newton's equation.

The motion of quasi-free electrons inside a metal is described classically. Quantum mechanical Coulomb correlations and exchange contributions are thus missing while the classical Coulomb interaction (i.e. the Hartree term in a quantum mechanical derivation) is fully included [8]. Furthermore, the Coulomb scattering due to higher-order quantum corrections is phenomenologically described via an inverse decay time $\gamma = 1/\tau$ [9, 10, 11]. The electrons inside the metal are approximated as a continuous fluid and macroscopic quantities such as electron number density n_e and electron velocity $\mathbf{u}_e$ are therefore continuous functions of position $\mathbf{r}$ and time t [12, 13]. The fluid satisfies the conservation of particle density which is described by the continuity equation

$$\frac{\partial n_e}{\partial t} + \nabla \cdot (n_e \mathbf{u}_e) = 0. \tag{1}$$

Under the excitation of an external EM wave with electric field $\mathbf{E}$ and magnetic field $\mathbf{B}$, the dynamics of the electron fluid is governed by the continuum generalization of Newton's equation,

$$m_e n_e \left(\frac{\partial}{\partial t} + \mathbf{u}_e \cdot \nabla \right) \mathbf{u}_e = -e n_e (\mathbf{E} + \mathbf{u}_e \times \mathbf{B}), \tag{2}$$

Here, m_e and $-e$ are the electron mass and charge, respectively. The so-called *convective* or *material* derivative of $\mathbf{u}_e$ on the left-hand side is a result of the description of electrons in terms of a continuous density and can be formally derived from the quantum mechanical Wigner distribution [8]. More intuitively, it can be understood as the time derivative of an electron taken with respect to a coordinate system which is itself moving with velocity $\mathbf{u}_e(\mathbf{r}(t), t)$, given by [12, 13]

$$\frac{d\mathbf{u}_e}{dt} = \frac{\partial \mathbf{u}_e}{\partial t} + \left[\frac{d\mathbf{r}(t)}{dt} \cdot \nabla \right] \mathbf{u}_e = \left(\frac{\partial}{\partial t} + \mathbf{u}_e \cdot \nabla \right) \mathbf{u}_e. \tag{3}$$

To describe the interaction between the electron fluid and the EM field self-consistently, the electron dynamics have to be coupled to Maxwell's equations. Consequently, it is convenient to express the charge density

*zengy@acms.arizona.edu
†The first and second author contributes equally to this article.

and the current density,

$$\rho(\mathbf{r},t) = e\left(n_i(\mathbf{r}) - n_e(\mathbf{r},t)\right), \tag{4}$$

$$\mathbf{j}(\mathbf{r},t) = (-e)n_e(\mathbf{r},t)\mathbf{u}_e(\mathbf{r},t), \tag{5}$$

in terms of the number density and the velocity field. Here, the ions are assumed to have an infinite mass such that only the electrons contribute to the electric current and the ion number density n_i is time-independent. By choosing n_i equal to a constant inside the metal and zero outside, the geometry of the metallic MM is fully described by $n_i(\mathbf{r})$.

Using the definitions from Eqs. (4) and (5) together with the differential Eqs. (1) and (2), we can derive equations for ρ and $\mathbf{j}$. The total set of these equations coupled to the EM fields via Maxwell's equations is known in plasma physics as the *cold-plasma wave equations* [12, 13]. The equations are

$$\nabla\cdot\mathbf{B} = 0, \tag{6}$$

$$\epsilon_0\nabla\cdot\mathbf{E} = \rho, \tag{7}$$

$$\nabla\times\mathbf{E} = -\frac{\partial\mathbf{B}}{\partial t}, \tag{8}$$

$$\nabla\times\mathbf{H} = \epsilon_0\frac{\partial\mathbf{E}}{\partial t} + \mathbf{j}, \tag{9}$$

$$\frac{\partial\mathbf{j}}{\partial t} = \sum_k \frac{\partial}{\partial r_k}\frac{\mathbf{j}j_k}{en_e} + \frac{e^2n_e}{m_e}\mathbf{E} - \frac{e}{m_e}\mathbf{j}\times\mathbf{B} - \gamma\mathbf{j}, \tag{10}$$

$$\frac{\partial\rho}{\partial t} = -\nabla\cdot\mathbf{j}. \tag{11}$$

In practice, the set of Eqs. (6)–(11) is redundant to a certain degree. For example, Faraday's law of induction, Eq. (8), automatically guarantees a vanishing divergence of $\mathbf{B}$ for all times if $\mathbf{B}$ is initially chosen divergence-free. In the same way, Eq. (9) along with Eq. (7) are equivalent to the continuity Eq. (11) [14]. Hence, only the reduced set of Eqs. (7)–(10) has to be solved.

By expanding the above equations in terms of the peak electric-field amplitude of the illuminating EM pulse, we can obtain two sets of equations [15, 16, 17]. The first set describes the linear-optical (first-order) response of a classical Drude-type metal whose permittivity is given by

$$\epsilon(\omega) = 1.0 - \frac{\omega_p^2}{\omega(\omega+i\gamma)}. \tag{12}$$

The second set, taking the linear fields ($\mathbf{E}_1$, $\mathbf{B}_1$ and $\mathbf{j}_1$) as sources, captures the second-order nonlinear-optical process of the metal,

$$\nabla\times\mathbf{E}_2 = -\frac{\partial\mathbf{B}_2}{\partial t}, \tag{13}$$

$$\nabla\times\mathbf{B}_2 = \frac{1}{c^2}\frac{\partial\mathbf{E}_2}{\partial t} + \mu_0\mathbf{j}_2, \tag{14}$$

$$\begin{aligned}\frac{d\mathbf{j}_2}{dt} &= \epsilon_0\omega_p^2\mathbf{E}_2 - \gamma\mathbf{j}_2 + \sum_k \frac{\partial}{\partial r_k}\frac{\mathbf{j}_1 j_{1,k}}{en_i} \\ &\quad - \frac{\epsilon_0 e}{m_e}\left(\nabla\cdot\mathbf{E}_1\right)\mathbf{E}_1 - \frac{e}{m_e}\mathbf{j}_1\times\mathbf{B}_1\end{aligned} \tag{15}$$

where the bulk plasma frequency $\omega_p(\mathbf{r})$ is defined by $\omega_p^2(\mathbf{r}) = e^2n_i(\mathbf{r})/\epsilon_0 m_e$ [16], and k represents x, y and z coordinate. The form of this set of equations immediately suggests: (i) its homogeneous part is exactly identical to the linear set such that the propagation of the generated SH wave is modified by the Drude response of the metal; and (ii) there are three distinct nonlinear sources for SHG in the plasma, representing different physical mechanisms. The second and third source are the well-known electric- and magnetic-component of the Lorentz force, respectively. The first source term is a generalized divergence originating from the convective time derivative of the electron velocity field $\mathbf{u}_e$ mentioned above.

For the numerical solution of the coupled differential Eqs. (13)–(15) and their linear counterparts, a three-dimensional finite-difference time-domain (FDTD) algorithm is applied. According to Yee's discretization scheme, the whole computational space is divided into millions of cubic grids [18]. Due to the translational symmetry in the xy plane it is sufficient to simulate a single unit cell of the periodic MM. Periodic boundary conditions are employed in the xy-direction while perfectly-matched layers are implemented in z-direction perpendicular to the metallic layer. The incoming electric field propagating along the $-z$ direction is generated by a total-field/scattering-field technique [18].

A variety of metallic MMs with different configurations have been studied numerically, and the details of these simulations will be discussed in a second publication [17]. From a detailed quantitative comparison between numerical simulations and experimental measurements, it is concluded that our simulations agree very well with the experimental observations [1, 2, 3]. For instance, we have confirmed the symmetry requirement that far-field SHG signals polarized along a direction of mirror symmetry are forbidden. Thus, a rectangular array of "U" or "T" structures can only show SHG in one polarization direction while SHG is absolutely forbidden from arrays of centro-symmetrical structures. Thus, our theory of the classical Coulomb-interacting electron gas catches the physical mechanism of SHG from metallic MMs.

In the following, we focus on arrays of metallic split-ring-resonators (SRRs) similar to those studied in Ref.[1]. Those materials are known to possess negative effective permeabilities in certain frequency regions and are generally referred to as magnetic MMs. A schematic drawing of a single unit cell of the periodic SRR array is shown in Fig.1. The complete structure then consists of a rectangular lattice of SRRs periodically arranged in the xy

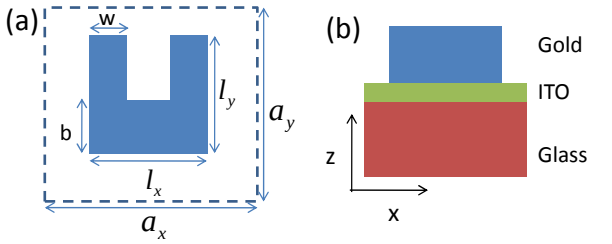

FIG. 1: (color). (a) Schematic drawing of a rectangle lattice of gold split-ring resonators. (b) There are three layers (gold, ITO and glass) along the z direction.

plane. The cross section of the structure in Fig. (1b) shows that the metallic layer is supported by a glass substrate coated with a thin film of indium-tin-oxide (ITO) in the z-direction. Furthermore, the SRRs are made of gold, and the thicknesses of the gold layer and the ITO film on the semi-infinite glass substrate are 25 nm and 5 nm, respectively.

To study the dependence of SHG on the different-order plasmonic resonances, two different-size SRRs are considered. The small one, named as S1, closely matches the small-SRR sample fabricated in Ref.[1], has lattice constants of the rectangle lattice $a_x = a_y = 305$ nm, the width of the metallic ring $w = 60$ nm, $l_x = l_y = 220$ nm and $b = 115$ nm. The big one, referred to as S2, resembles S1 graphically and takes geometric parameters as follows: $a_x = 610$ nm, $a_y = 635$ nm, $l_x = 455$ nm, $l_y = 470$ nm, $w = 135$ nm and $b = 95$ nm. In addition, the permittivity of the ITO layer and glass substrate is 3.8 and 2.25, respectively. The bulk plasma frequency of gold is taken as $\omega_p = 1.367 \times 10^{16} s^{-1}$, and the phenomenological collision frequency $\gamma = 6.478 \times 10^{13} s^{-1}$ [5, 6]. The sizes are chosen such that both structures have a resonance around a wavelength of 1500 nm. For the purposes of physical clarity, S2 is slightly different from the big-SRR sample in Ref.[1], and geometrically identical to S1. We will show below that this disagreement does not influence our conclusions qualitatively.

Our main results are plotted in Fig.2. Firstly, we study the linear-optical properties of these magnetic MMs. The transmitted and reflected spectra under illuminating light with different polarization are calculated and presented. Our numerical spectra agree qualitatively and quantitatively with the experimental spectra in Ref.[1]. Our main interest is the transmission null around 1502-nm wavelength of S1, and we discuss its physical mechanism in detail. As already pointed out, such a transmission null is a sign of the fundamental plasmonic resonance (its mode distribution is shown in Fig.(3a)), which is induced by the oscillation of circulating currents inside the metallic rings. This plasmonic resonance bears an analogy to an inductor-capacitor circuit resonance. It is consequently mainly determined by the inductance of the loop and the capacitance of the SRR gap. On the

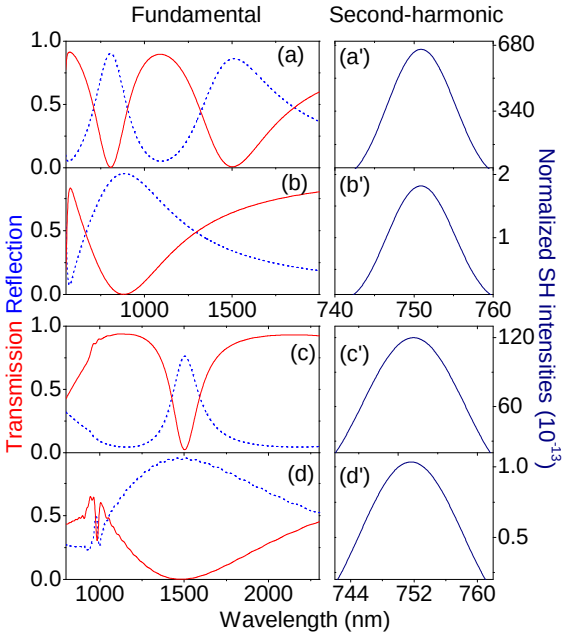

FIG. 2: (color). Summary of the linear-optical spectra and normalized second-harmonic intensities for two magnetic metamaterials, S1 and S2. Both transmission (solid) and reflection (dashed) spectra are plotted. The wavelength of the illuminating fundamental-frequency wave is fixed at 1502 nm. The metamaterial S1 is excited by (a,a') x- and (b,b') y-polarized incidence. The metamaterial S2 is excited by (c,c') x- and (d,d') y-polarized incidence. The polarization of the generated second-harmonic waves from both metamaterials are only allowed in the y direction.

other hand, the transmission null of S2 results from the second-order plasmonic resonance whose mode is characterized as a single-node standing wave around the SRR metallic ring [7, 17], as can be found from its near-field distribution plotted in Fig.(3b).

Next we study SHG from these magnetic MMs illuminated by a fundamental-frequency (FF) wave with wavelength of 1502 nm as well as peak electric-field amplitude of 2×10^7 (V/m) (same as that employed in the experiments [1, 2]). In order to describe the energy conversion efficiency in this nonlinear-optical process, we define a normalized SH intensity,

$$\eta = \frac{|\mathbf{E}_2(2\omega_0)|^2}{|\mathbf{E}_1(\omega_0)|^2}, \tag{16}$$

to measure the strength of the far-field negative z-propagating SH wave, where ω_0 is the frequency of the incident FF wave. Because the infinite-thickness glass substrate is utilized here, the true SH conversion efficiency equals η times $\sqrt{\epsilon_{\text{glass}}}$ [16]. Two important conclusions can be observed from Fig.2:

(1) Because these magnetic MMs possess x-coordinate mirror symmetry, only a y-polarized SH wave can be ex-

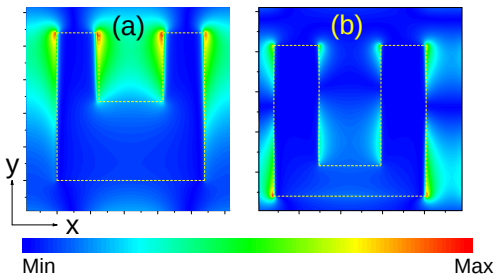

FIG. 3: (color). Magnitude ($|E_x|$) distributions of (a) the fundamental plasmonic resonance of S1 and (b) the second-order plasmonic resonance of S2, at a distance of 5 nm above the gold film. Dashed lines mark the positions of the gold split-ring-resonators.

cited by either x- or y-polarized incident fields. Such an incidence-polarization dependence was already experimentally observed [1, 2, 3]. Moreover, a universal selection rule can be extracted from all our numerical simulations [17], that is, a mirror symmetry of the metallic MM in one direction completely prohibits SHG in the same direction.

(2) As shown in Fig.($2a'$), the strongest SHG signal with a normalized SH intensity of 6.7×10^{-11} is achieved due to the excitation of the fundamental plasmonic resonance of S1 by x-polarized incidence. As a reference, the corresponding experimental observation is roughly 2.0×10^{-11} [2, 3]. We now normalize this signal to 100% and relate all other signals to it.

For excitation of the second-order plasmonic resonance with x-polarized illumination in Fig.($2c'$), a relatively significant SH emission is observed from S2 with normalized SH intensity of 18%. (An MM which closely matches the big-SRR sample in Ref.[1] provides an SH signal of 7.8% [17], quite close to the experimental measurement 4.3%). On the other hand, only weak SH signals with 0.2% intensities are found from the off-resonance configurations, as shown in Fig.($2b'$,$2d'$). Therefore, the presence of plasmonic resonances and thus circulating currents can greatly enhance SHG from magnetic MMs. Moreover, different-order plasmonic resonances make different contributions. The fundamental resonance contributes about fourfold to the second-order resonance. It can be interpreted by the localization degree of the linear field, because such a compression can enhance SHG even without perfect phase matching [16, 19]. As shown in Fig.3, the linear electric fields of both resonances are localized inside the SRR gap, and the stronger compression appears for the fundamental plasmonic resonance.

Now we try to distinguish the dominant source among these nonlinear terms for S1 on resonance. By numerically switching off these sources one by one, their respective contribution can be roughly estimated. The magnetic Lorentz force, $\mathbf{j} \times \mathbf{B}$, makes a weak contribution as small as 2%. Its electric counterpart provides 29%. The most significant contribution, 68%, comes from the convective derivation of current. The sum of the last two terms, consequently, constructively dominates SHG emission from magnetic MMs. It is further found that, the contribution of the magnetic Lorentz force is negligible as long as the structural fundamental plasmonic resonance is excited [17]. Such an observation is quite different from the previous interpretations, in which the magnetic contribution was emphasized [1].

In conclusions, a classical theory of second-harmonic generation from magnetic metamaterials is presented in this Letter. The quasi-free electrons inside the metallic nanostructure are approximated as a classical Coulomb-interacting electron gas, and their motion under the excitation of an external electromagnetic field is described by the cold-plasma wave equations. Through numerical simulations, it is demonstrated that the classical theory includes the dominant physical mechanisms both qualitatively and quantitatively. It is further shown that: (1) A mirror symmetry of metamaterial in one direction completely prohibits the generation of far-field second-harmonic wave in the same direction; (2) The presences of structural plasmonic resonances can significantly enhance second-harmonic generation; (3) As long as the lowest-order plasmonic mode is excited, the magnetic Lorentz force makes negligible contribution to second-harmonic generation.

We thank Prof. Martin Wegener and his group in Universität Karlsruhe, Dr. Jens Förstner of Paderborn University, Prof. Moysey Brio, Dr. Miroslav Kolesik and Dr. Colm Dineen of University of Arizona for their invaluable discussions. This work is supported by the Air Force Office of Scientific Research (AFOSR), under Grant No. FA9550-07-1-0010 and FA9550-04-1-0213. J. V. Moloney acknowledges support from the Alexander von Humboldt.

[1] M. W. Klein, C. Enkrich, M. Wegener, S. Linden, Science 313, 502 (2006).
[2] M. W. Klein, M. Wegener, N. Feth, S. Linden, Optics Express 15, 5238 (2007).
[3] N. Feth, S. Linden, M. W. Klein, M. Decker, F. Niesler, and M. Wegener, Optics Lett. submitted.
[4] J. B. Pendry, A. J. Holden, D. J. Robbins, W. J. Stewart, IEEE Trans. Microwave Theory Tech. 47, 2075 (1999).
[5] S. Linden, C. Enkrich, M. Wegener, J. Zhou, Th. Koschny, C. M. Soukoulis, Science 306, 1351 (2004).
[6] C. Enkrich, M. Wegener, S. Linden, S. Burger, L. Zschiedrich, F. Schmidt, J. F. Zhou, Th. Koschny, and C. M. Soukoulis, Phys. Rev. Lett. 95, 203901 (2005).
[7] C. Rockstuhl, F. Lederer, C. Etrich, Th. Zentgraf, J.

Kuhl, and H. Giessen, Opt. Express 14, 8827 (2006).
[8] W. Hoyer, J. V. Moloney, E. M. Wright, M. Kira, S. W. Koch, J. Phys: Conference series, 11, 153 (2005); W. Hoyer, A. Knorr, J. V. Moloney, E. M. Wright, M. Kira, S. W. Koch, Phys. Rev. Lett. 94, 115004 (2005).
[9] S. S. Jha, Phys. Rev. Lett. 15, 412 (1965).
[10] S. S. Jha, Phys. Rev. 140, A2020 (1965).
[11] N. Bloembergen, R. K. Chang, S. S. Jha, C. H. Lee, Phys. Rev. 174, 813 (1968).
[12] T. J. M. Boyd, J. J. Sanderson, *The physics of plasmas* (Cambridge, 2003).
[13] J. Freidberg, *Plasma Physics and Fusion Energy* (Cambridge, 2007).
[14] M. Born and E. Wolf, *Principle of Optics* (Seven Edition, Cambridge, 1999).
[15] J. E. Sipe, V. C. Y. So, M. Fukui, and G. I. Stegeman, Phys. Rev. B 21, 4389 (1980).
[16] Y. R. Shen, *The principles of Nonlinear Optics* (John Wiley & Sons, New York, 1984).
[17] Y. Zeng, W. Hoyer, J. Liu, S. W. Koch, J. V. Moloney, to be submitted.
[18] A. Taflove and S. C. Hagness, *Computational Electrodynamics: the finite-difference time-domain method* (Second Edition, Artech House, Boston, 2000).
[19] Y. Zeng, X. Chen, W Lu, J. Appl. Phys. 99, 123107 (2006).